

Performance analysis and optimization for a novel air-source gas-fired absorption heat pump

Zhangxiang Wu ^{a,b}, Shijun You ^{a,b}, Huan Zhang ^{a,b}, Yaran Wang ^{a,b,*}, Shen Wei ^c, Yan Jiang ^a, Tingting Jiang ^a, Li Sha ^a

^a School of Environmental Science and Engineering, Tianjin University, Tianjin, 300350, PR China

^b Tianjin Key Lab of Biomass/Wastes Utilization, Tianjin 300350, PR China

^c The Bartlett School of Construction and Project Management, University College London (UCL), 1-19 Torrington Place, London WC1E 7HB, United Kingdom

ABSTRACT: In district heating technologies, gas fired boilers and conventional heat pumps have poor performance at low ambient temperature. To tackle this issue, this study has proposed a novel air-source gas-fired absorption heat pump for district heating with flue gas recovery. Compared with conventional absorption heat pumps, the proposed solution in this study can absorb heat from both air and flue gas. Additionally, the working fluid works properly when air temperature is below 0 °C, safe and nonflammable. To analyze the economic and the thermodynamic performance of this air-source gas-fired absorption heat pump, a mathematical model, considering energy, exergy, economy and environment, has been developed. According to the simulation results of the model, the proposed air-source gas-fired absorption heat pump system here had good stability and feasibility under various operational conditions. However, as the payback period and the exergy destruction were found to be conflicting with each other, a multi-objective optimization method was established to minimize the system's payback period and exergy destruction simultaneously. Additionally, the technique for order preference by similarity to an ideal solution decision-making method has been applied to look for the optimal solutions in the Pareto frontier, with optimal solutions of the system under different operational conditions recommended.

KEYWORDS: absorption heat pump; mathematical model; thermodynamic analysis; multi-objective optimization

Nomenclature		<i>t</i>	temperature (°C)
<i>A</i>	area (m ²)	<i>T</i>	temperature (K)
AHP	absorption heat pump	TOPSIS	technique for order preference by similarity to an ideal

AGAHP	air-source gas-fired absorption heat pump	solution
		$\square T_{LMTD}$ logarithmic mean temperature difference
A_n, B_n, C_n, G_n	constant coefficient	U overall heat transfer coefficient [W/(m ² ·K)]
COP	coefficient of performance	W power (kW)
CRF	capital recovery factor	Y molar concentration (%)
\dot{C}_{in}	input cost rate (\$/s)	\dot{Z}_{op} cost rate of operating (\$/s)
\dot{C}_g	gas cost rate (\$/s)	\dot{Z}_k capital investment rate and maintenance costs (\$/s)
\dot{C}_{env}	environment cost rate (\$/s)	Subscript
C_{total}	total cost (\$)	abs absorber
c_{CO_2}	cost of CO ₂ avoided (\$/ton)	a Air
c_p	constant pressure specific heat of water (kJ/kg·K)	c cold
Cl_i	proximity index	cond condenser
EC	system annual electrical energy consumption (kWh)	env environment
EP	average of electricity price in China (\$/kWh)	evap evaporator
EEV	electronic expansion valve	fue fuel
$\dot{E}x$	exergy rate (kW)	g gas
$\square ED$	exergy destruction rate (kW)	gen generator
HP	average of heat price in China (\$/kWh)	h hot
ΔH_m	the heat of mixing of the R22-DEGDME (J/mol)	he heat exchanger
H	molar enthalpy (kcal/kg)	in inlet
h	specific enthalpy (kJ/kg)	op operating
i	annual interest rate (%)	out outlet
J	heat equivalent of work (kg·m/kcal)	R refrigerant
m	mass flow rate (kg/s)	s strong
MOP	multi-objective optimization	sys system
M	molecular weight (g/mol)	w weak
N	annul operating hour (h)	
n	system life time (year)	Greek symbols
P	pressure (MPa)	μ_{CO_2} emission factor (kg/kWh)

P_{sp}	power input (kW)	ψ	exergy efficiency
PP	payback period (year)	ϕ	maintenance factor
Q	heat transfer rate (kW)	η_b	Boiler efficiency
s	specific entropy [kJ/(kg·K)]		
SOP	single-objective optimization		

1. Introduction

Nowadays, space heating heavily relies on burning fossil fuels, which include natural gas, petroleum and coal. The massive use of fossil fuels, however, has brought serious pollution and haze issues. To ease these issues in China, the Chinese government has changed the fuel of thermal power plants from coal to gas. This, however, brings new issues such as gas shortage and greenhouse gas release [1]. With the continued increase of both population and economy, many studies have focused on utilizing renewable energy, and many researchers believed that air source energy is a reliable and environmental-friendly energy source for future buildings [2].

Mahdi et al. [3] have studied an air source heat pump solution, working as a waste heat recovery system, with a thermo-economic-environmental model developed to analyze the system's benefits. Qiu et al. [4] evaluated the energy performance of a low-GWP (Global Warming Potential) refrigerant in an air-source heat pump for heating. Based on load balance, Li et al. [5] proposed a dynamic coupling selection method for air-source heat pumps. Although the compression heat pump has been widely used in some cold regions and the coefficient of performance (COP) can reach about 3, the efficiency of power generation at the thermal power plants has not been considered when calculating this value [6]. In addition, air source absorption heat pumps have been studied as well due to its advantages, like environmental friendliness, energy efficiency and low investment. Wu et al. [7] have proposed a solar air source absorption heat pump system and suggested its best working configurations. Compared with conventional direct solar heating systems, the proposed system gave a better performance and generated fewer pollutants. Dai et al. [8] have investigated an air source ammonia-water absorption heat pump, which used solar energy and natural gas as heat sources. The system's COP was found to be between 1.44 and 1.66, with evaporating temperature between 4.3 °C and 11.1 °C. Additionally, they also built a mathematical model of the system and found the operational cost of this system can be reduced with additional solar collectors. Li et al. [9] have proposed an air source absorption heat pump system for heating and established a simple model based on mass and heat balances. The model was validated against previous references and the use of this model has demonstrated great energy saving potential of the proposed system in actual application. Wu et al. [10] have investigated the performance of an air source absorption heat pump using energy models and identified its energy saving rate, efficiency and distribution consumption.

Christopher et al. [11] have developed a thermodynamic model for a direct gas-fired single effect ammonia-water absorption heat pump, and suggested its optimization configurations for heating. Lu et al. [12] have designed and proposed an air source ammonia-water absorption heat pump system, which could absorb heat from ambient and exhaust gas. Their experimental results showed that at evaporating temperature of 0 °C this solution could provide 30 kW heat with a COP of 1.66, and it was a more energy efficient than conventional district heating solutions.

As absorption heat pumps contribute a lot to energy conservation and emission reduction, many studies have been done at both theoretical and practical levels. Wang et al. [13] presented a cascaded absorption heat pump to utilize industrial waste heat, and analyzed its exergy and exergoeconomic performance to determine the solution's Exergy Destruction (ED) and cost rates. From the study, they suggested that 21.3 % exergy destruction rate could be avoidable by improving heat exchangers, with 80.2 % investment cost due to components of heat exchangers. Luca et al. [14] proposed a reversible absorption heat pump with internal combustion engine, for trigeneration systems. They carried out both exergy and energy analyses to evaluate the solution's economic viability and thermodynamic performance, and found that compared with conventional systems, the exergy and cost savings of the proposed system could reach 43 % and 10 %, respectively. Li et al. [15] proposed a co-generation system coupled with absorption heat pumps, with mathematical models developed for energy and exergy analysis. Lu et al. [6] introduced a novel absorption heat pump system with cascaded recovery of flue gas, and established a simulation model based on the Aspen Plus to analyze the exergy, energy and economic performance of the system. It was suggested that the proposed system had a heat capacity up to 50 kW.

The exergy and energy analyses are helpful for improving the thermodynamic performance of the system but may increase capital investment and payback period. Therefore, optimization of absorption heat pump systems considering both thermodynamic and economic performances should be conducted. Bellos et al. [16] have proposed an absorption heat pump system for both heating and cooling, and optimized its performance based on thermodynamic parameters. Rodrigue et al. [17] have proposed a three-heat-reservoir absorption heat pump system with exergy, ecological and thermo-economic analysis, in order to find the optimal operational conditions for the system with minimized exergy loss, capital cost and environmental impact. From the study, they found that high thermo-economic criterion would give low investment but high energy cost. Vinther et al. [18] have investigated a district heating plant including four water-lithium bromide (H₂O-LiBr) absorption heat pumps using micro-genetic algorithms for optimization. Jia et al. [19] presented an ammonia-water absorption-resorption heat pump and developed a mathematical model to identify feasible high and low pressures. Additionally, they compared heat source temperature demand and inner operation pressure with conventional absorption heat pumps and identified optimal solutions. Vaibhav et al. [20] conducted energy, exergy and economic analysis for an absorption heat transformer with water-lithium bromide as working fluid, and found that there was a conflict between the economic

and thermodynamic performances. Additionally, the operational parameters could be determined by non-dominated sort genetic algorithm-II (NSGA-II) technique of multi-objective optimization (MOP), with results showing that MOP design had a better performance than the single-objective optimization (SOP) design.

The review work on these studies can reveal that both energy, exergy, economic analysis and optimization of absorption heat pumps have been conducted in many existing studies. There is, however, still a lack of knowledge of air-source gas-fired absorption heat pumps (AGAHP) considering energy, exergy, economic and environmental analysis with multi-objective optimization. Unlike previous optimization studies on the absorption heat pump which focus solely on the energy analysis and exergy analysis, the economic analysis, environmental analysis, the mathematical model of R22-DEGDME (Diethylene Glycol Dimethyl Ether) and the MOP of the system have not been sufficiently discussed in the open literatures yet. Appropriate optimization strategies are necessary to put forward to improving the performance of AGAHP from the sights of economy and environment. Therefore, this paper firstly elaborated the basic functions of AGAHP, with R22-DEGDME selected as working fluid. A mathematical model has been developed for the proposed system, with considerations in terms of thermodynamic, economic and environmental performances. In addition, as there was a conflict between payback period and exergy destruction, the optimal system performance was obtained based on the MOP. An optimization method for AGAHP system based on NSGA-II technology and TOPSIS (Technique for Order Preference by Similarity to an Ideal Solution) decision-making method was also established to identify optimal results. The main contributions of this study include:

- (1) The energy, exergy, economy and environment performance of a novel air-source gas-fired absorption heat pumps under different operating conditions were analyzed.
- (2) A mathematical model of R22-DEGDME solution was established.
- (3) Based on the simulation results, multi-objective optimization of the system was conducted and some optimal operational conditions were recommended.

2. System description

Fig. 1 shows the schematic of the AGAHP, with five branches including refrigerant, weak solution, strong solution, gas and water branches. The main components of this system are one solution heat exchanger, one generator, one solution pump, one absorber, one evaporator, one reservoir, one condenser and three heat exchangers.

The water branch is illustrated by blue lines, where the return water from the user is pumped to the absorber, absorbing heat from the solution. It then enters the condenser and absorbs heat from the high temperature refrigerant vapor. The water finally passes the heat exchanger-I and then is supplied to the user. The gas branch is represented by red lines. A mixture of air and natural gas is supplied to the combustor and the heat is then released to the solution in the generator. The flue gas from the combustion process goes to the heat exchanger-I to warm up the supply water. The

gas then enters the heat exchanger-II and the temperature can be further reduced to below the dew point, so the waste heat can be recovered by low temperature refrigerant vapor. Finally the exhaust gas is released into the atmosphere.

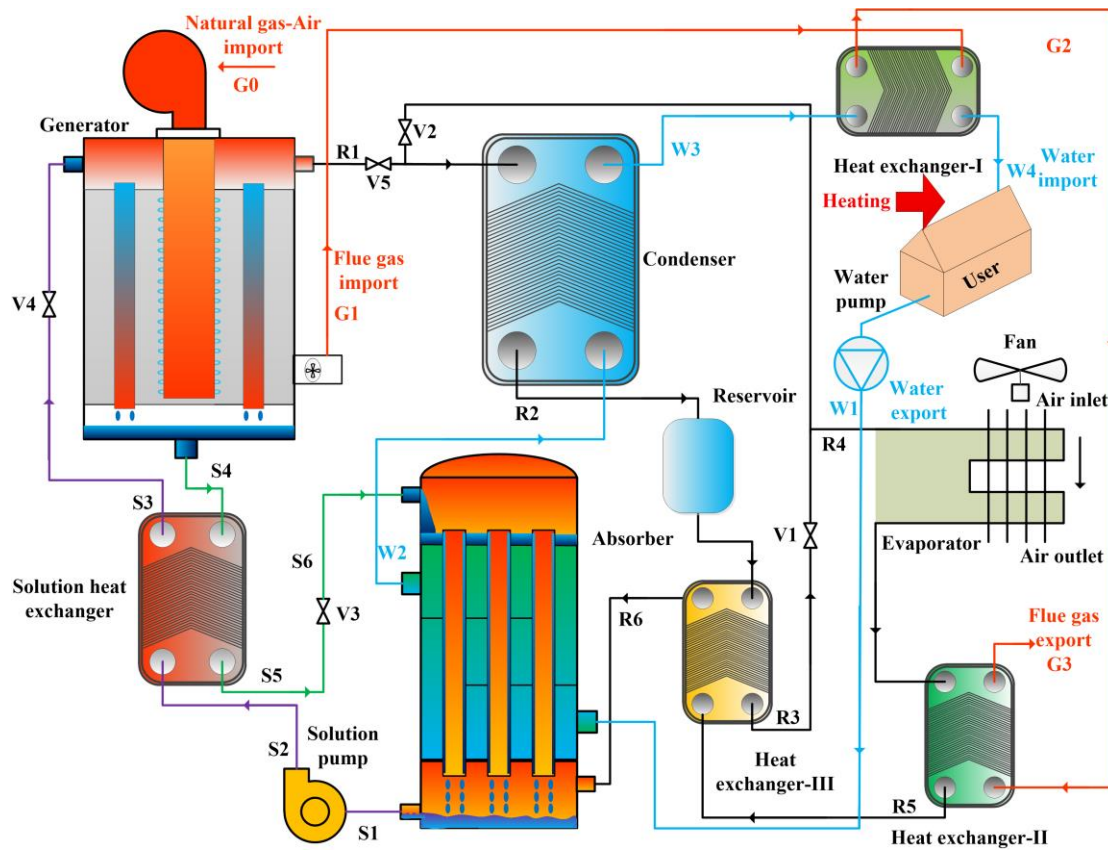


Fig.1 Schematic diagram of the AGAHP

The strong solution and weak solution branches are represented by purple and green lines, respectively. The strong solution from the absorber is pumped to the solution heat exchanger by the solution pump, leading to increased solution pressure. The strong solution absorbs heat from the weak solution in the solution heat exchanger and then enters the generator. In the generator, the strong solution is heated by the combustion of natural gas to generate refrigerant vapor. The strong solution then becomes weak solution and enters the solution tank. The weak solution goes into the solution heat exchanger, then the Electronic Expansion Valve (EEV) and finally returns to the absorber. In the absorber, the low temperature refrigerant vapor is absorbed by the weak solution, releasing much heat to the water. The weak solution finally turns to strong solution and enters the solution pump.

The refrigerant branch is shown by black lines. In this process, high temperature refrigerant vapor generated in the generator enters the condenser and heats the water. It then goes to the reservoir, the heat exchanger-III and the EEV, and then turns to low temperature-pressure refrigerant liquid. In the evaporator, the liquid evaporates by absorbing heat from the air source and the vapor goes into the absorber after the heat exchanger-III. In addition, when defrosting is necessary, the valve-II will be opened

so high temperature refrigerant vapor goes into the evaporator directly.

To improve the efficiency of this system, the waste heat in the flue gas was analyzed. Combustion of gas will generate CO_2 , N_2 and H_2O . To ensure complete combustion, surplus air is necessary, which can be quantified by excess air coefficient α . The combustion reaction of gas and air process is shown as:



As shown in Fig. 2, boiler efficiency increases with decreasing flue gas temperature for different excess air [21]. Boiler efficiency rises slowly before the dew point and then it starts to increase sharply with decreasing flue gas temperature. When flue gas temperature is higher than dew point, its cooling process releases sensible heat with less amount [6]. When the temperature is lower than the dew point, however, there is abundant energy of latent heat, leading to great increase of boiler efficiency.

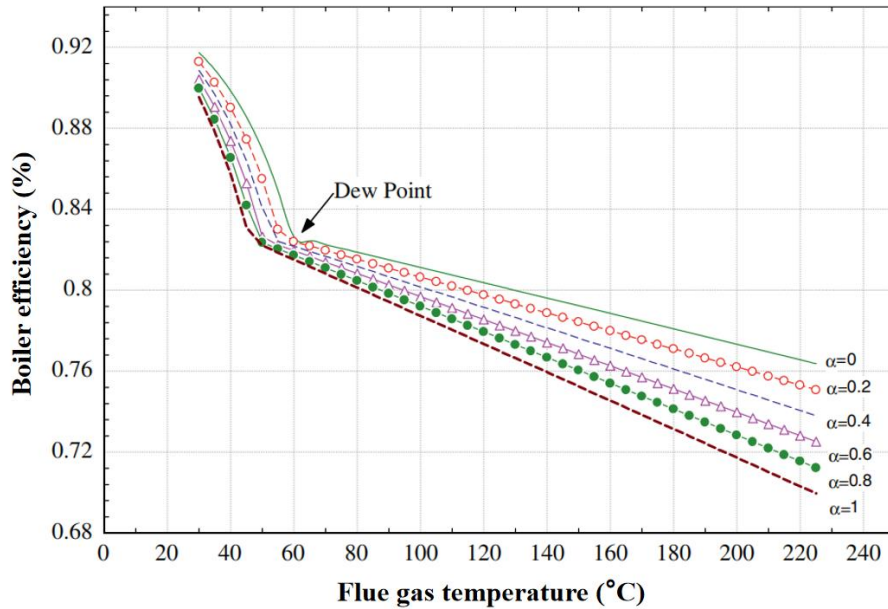


Fig. 2 Variation of boiling efficiency with different excess air and flue gas temperature [21]

To reduce irreversible loss and improve thermodynamic efficiency, refrigerant and solution need to be suitably selected. Although many studies have tried to use ammonia-water and water-lithium bromide pairs for absorption heat pumps, they have certain shortcomings: 1) ammonia is toxic and flammable, and 2) water-lithium bromide absorption heat pump cannot work with evaporation temperatures below 0 °C [22, 23]. In this study, therefore, R22-DEGDME solution was selected because it was nontoxic and nonflammable, and could work below 0 °C [24]. Despite the fact that there are some negative effects on the environment with ozone problem and global warming, this solution provides a better efficiency, application and useful knowledge [25,26]. The properties of R22-DEGDME are shown in Table 1.

Table 1 The properties of R22-DEGDME [25]

Parameters	R22	DEGDME
------------	-----	--------

Molecular weight (g/mol)	86.46	134.17
Boiling point (°C) (P=0.101 MPa)	-40.8	162
Critical temperature (°C)	96.15	328.85
Density (kg/m ³) (t=20 °C)	1210	944
Toxicity	No	No
Corrosivity	No	No

3. Methods

To analyze the performance of the AGAHP, a mathematical model was developed to describe solution, energy, exergy, economy and environment. For simplification, some assumptions have been adopted in the modeling work:

1. The system operates at steady state.
2. The R22-DEGDME solution is saturated at the exits of both the generator and the absorber.
3. The refrigerant at the outlets of the evaporator and the condenser outlets are saturated.
4. The heat dissipation of the equipment and pipes to the surroundings can be ignored.
5. The power input of the evaporator fan is neglected.
6. The reference state temperature and the pressure in the exergy analysis were 298.15 K and 101.32 kPa, respectively.

3.1. Solution analysis

The solution balance consists of pressure, molar concentration and temperature, and can be expressed by [Equation 2 \[25,27\]](#).

$$\ln P = \sum_{n=0}^5 A_n Y^n + \frac{1}{T} \sum_{n=0}^5 B_n Y^n + \ln T \cdot \sum_{n=0}^5 C_n Y^n \quad (2)$$

where P is the pressure of the solution and Y is the molar concentration of R22. Constant coefficients, A_n , B_n and C_n , are shown in the [Table 2](#).

Table 2 Values for Coefficients in [Equation 2](#)

n	A_n	B_n	C_n
0	5.21E+01	-5.58E+03	-6.34E+00
1	1.27E+01	3.39E+03	-1.43E+00
2	-1.39E+02	-8.60E+03	2.23E+01
3	7.32E+02	-3.16E+03	-1.14E+02
4	-1.19E+03	3.04E+04	1.81E+02
5	5.47E+02	-1.90E+04	-8.19E+01

The specific heat of the R22-DEGDME solution can be calculated by Equation 3 [25,27].

$$c_p = \sum_{n=0}^3 A_n^{c_p} Y^n + t \sum_{n=0}^3 B_n^{c_p} Y^n + t^2 \cdot \sum_{n=0}^3 C_n^{c_p} Y^n \quad (3)$$

The constant coefficients $A_n^{c_p}$, $B_n^{c_p}$ and $C_n^{c_p}$ are shown in the Table 3.

Table 3 Values of Coefficients in Equation 3

n	$A_n^{c_p}$	$B_n^{c_p}$	$C_n^{c_p}$
0	2.79E+02	-4.2E-02	2.31E-03
1	-1.51E+02	5.98E-01	-5.97E-03
2	1.01E+02	-1.37E+00	3.43E-03
3	-1.28E+02	1.02E+00	1.05E-03

The mixed heat of R22 and DEGDME can be described by Equation 4 [25,27].

$$\Delta H_m = Y(1-Y) \cdot \sum_{n=1}^4 G_n (1-2Y)^{n-1} \quad (4)$$

where G_n is the constant coefficient, with values listed in Table 4.

Table 4 Values of Coefficients in Equation 4

n	G_n
1	-1.90E+04
2	8.72E+03
3	-1.39E+03
4	-6.42E+02

The molar enthalpy of the solution can be obtained by Equation 5 [25,27].

$$H = \frac{\Delta H_m + \int_0^t c_p dt + \int_0^{10} c_p(Y=0) dt + Y \left(\int_0^{10} c_p(Y=1) dt - \int_0^{10} c_p(Y=0) dt \right)}{J(M_D(1-Y) + M_{R22}Y)} + 100 \quad (5)$$

where J is the heat equivalent of work, M_D and M_{R22} are the molecular weights of DEGDME and R22, respectively. $c_p(Y=0)$ and $c_p(Y=1)$ are the specific heat when the molar concentrations are zero and one, respectively.

3.2. Energy analysis

The energy analysis was carried out based on the first and second laws of the thermodynamics. In the evaporator, condenser, solution heat exchanger and heat exchanger-I, the heat loads were calculated by [Equations 6 to 9](#), respectively.

$$Q_{evap} = m_r (h_{R5} - h_{R4}) \quad (6)$$

$$Q_{cond} = m_r (h_{R1} - h_{R2}) \quad (7)$$

$$Q_{she} = m_w (h_{S3} - h_{S2}) \quad (8)$$

$$Q_{he-I} = c_{p,w} m_w (T_{W4} - T_{W3}) \quad (9)$$

In the generator, the heat is transferred from the gas combustion to the strong solution, with heat load calculated by [Equation 10](#).

$$Q_{gen} = m_r \cdot h_{R1} + m_w \cdot h_{S4} - m_s \cdot h_{S3} \quad (10)$$

In the absorber, the heat released from the weak solution and the refrigerant vapor is absorbed by the water, and it can be described by [Equation 11](#).

$$Q_{abs} = m_r \cdot h_{R6} + m_w \cdot h_{S6} - m_s \cdot h_{S1} \quad (11)$$

The COP of the system can be calculated as the ratio of the heat capacity to heat consumption, as defined by [Equation 12](#).

$$COP = (Q_{cond} + Q_{abs} + Q_{he-I}) / (Q_{gen} / \eta_b + P_{sp}) \quad (12)$$

The above energy and solution models were developed in MATLAB to simulate the performance of the AGAHP system, following the flow chart depicted in [Fig. 3](#).

According to [\[25\]](#), the pressure differences ΔP_{R1-R2} , ΔP_{R5-R6} , ΔP_{R6-R1} , ΔP_{S2-S3} ,

ΔP_{S3-S4} , ΔP_{S4-S5} , ΔP_{R2-R3} , ΔP_{R4-R5} in the model were initialized as 0.20 bar, 0.05

bar, 0.10 bar, 0.20 bar, 0.05 bar, 0.10 bar, 0.05 bar and 0.15 bar, respectively.

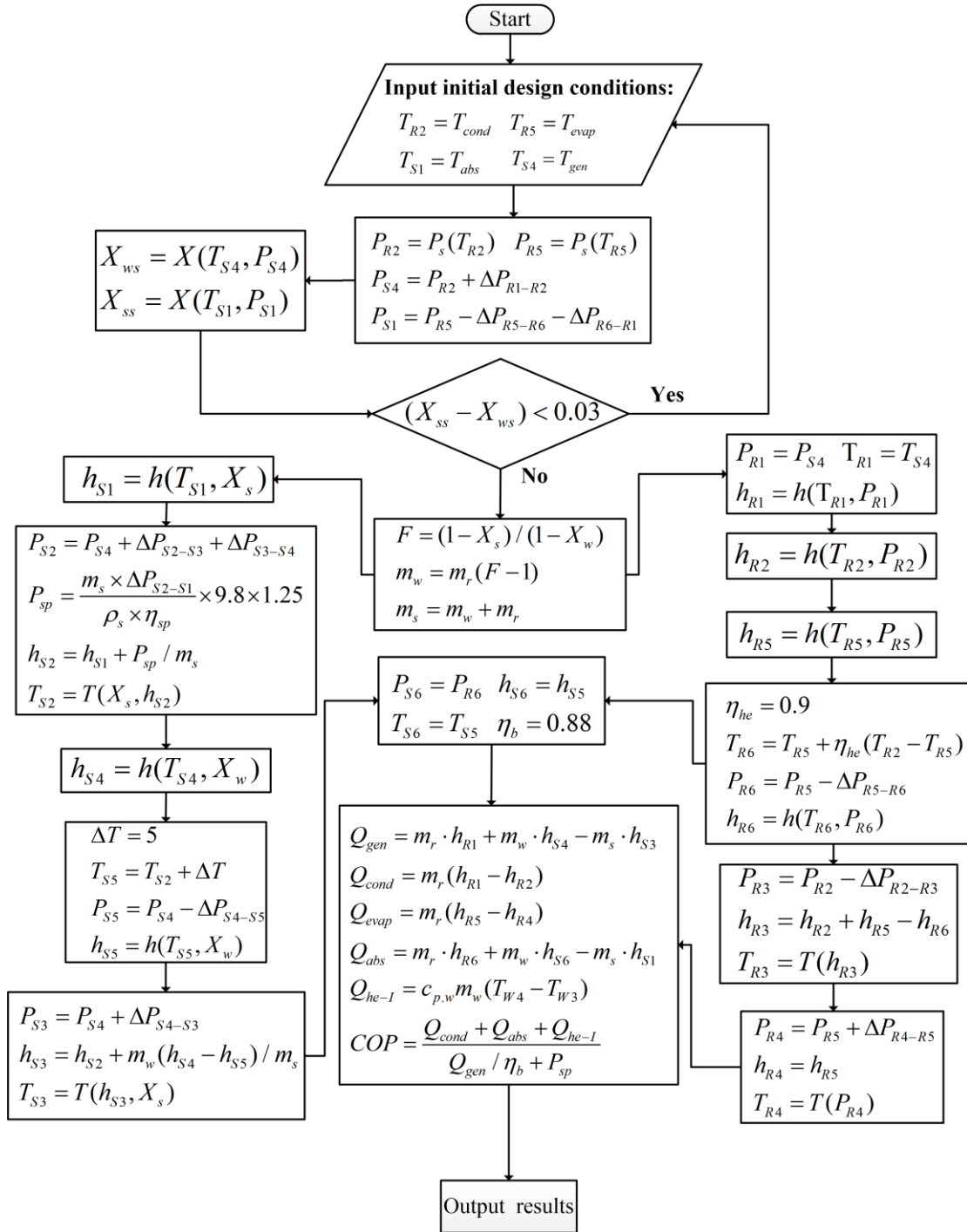


Fig. 3 The flow chart of energy and solution simulation

3.3. Exergy analysis

The exergy analysis is useful for identifying the maximum potential work of a given measure point with respect to the reference state. It can also specify the exergy destruction and show the reasons of thermodynamic imperfection [28]. There are four parts of exergy which are physical exergy, chemical exergy, kinetic exergy and potential exergy. Kinetic exergy and potential exergy are neglected and the exergy rate of the AGAHP system proposed in this study at any state point can be expressed by

Equation 13.

$$\dot{E}x_i = \dot{E}x_i^{ph} + \dot{E}x_i^{ch} \quad (13)$$

The chemical exergy of natural gas is equal to the maximum work obtainable through a process that converts the natural gas from the ambient state to the dead state. In this study, the chemical exergy of flue gas is ignored and only the input chemical exergy of natural gas ($\dot{E}x_{g,in}^{ch}$) is considered as 24 kW. The physical exergy can be written as:

$$\dot{E}x_i^{ph} = \dot{m}[(h - h_0) - T_0(s - s_0)] \quad (14)$$

Exergy destruction is related to the irreversible loss of the system, which can be expressed calculated by Equation 15.

$$ED = \sum \dot{E}x_{in} - \sum \dot{E}x_{out} - \sum \dot{W} + \sum (1 - \frac{T_0}{T}) \dot{Q} \quad (15)$$

where T is entropy-averaged temperature and can be determined by Equation 15[29].

$$T = \frac{h_{out} - h_{in}}{s_{out} - s_{in}} = \frac{T_{in} - T_{out}}{\ln(\frac{T_{in}}{T_{out}})} \quad (16)$$

Exergy efficiency is applied to evaluate the system's performance, calculated as the ratio of the output exergy rate to the input exergy rate, in Equation 17.

$$\psi_{sys} = \frac{\dot{E}x_{out}}{\dot{E}x_{in}} \quad (17)$$

where output and input exergy rates were defined by Equations 18 and 19, respectively.

$$\dot{E}x_{out} = \dot{E}x_{w,out}^{ph} + \dot{E}x_{a,out}^{ph} \quad (18)$$

$$\dot{E}x_{in} = \dot{E}x_{g,in}^{ch} + \dot{E}x_{w,in}^{ph} + \dot{E}x_{ai,in}^{ph} + \dot{P}_{sp} \quad (19)$$

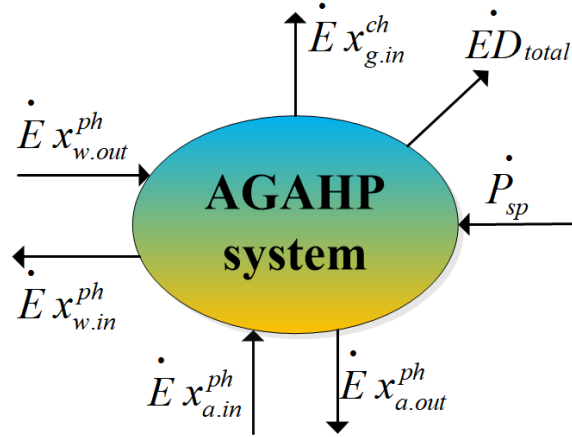


Fig. 4 Exergy analysis of the AGAHP system

The exergy efficiency of the AGAHP was then defined by Equation 20, with governing equations of main equipment shown in Table 5.

$$\psi_{sys} = \frac{\dot{E}x_{w,out}^{ph} + \dot{E}x_{a,out}^{ph}}{\dot{E}x_{g,in}^{ch} + \dot{E}x_{w,in}^{ph} + \dot{E}x_{a,in}^{ph} + P_{sp}} \quad (20)$$

Table 5 Governing equations of exergy analysis

Component	Equation	Exergy efficiency
Generator	$\dot{E}x_{g,in}^{ch} + \dot{E}x_{S3}^{ph} = \dot{E}x_{S4}^{ph} + \dot{E}x_{R1}^{ph} + \dot{E}D_{gen}^{ph}$	$\psi_{gen} = \frac{\dot{E}x_{S4}^{ph} + \dot{E}x_{R1}^{ph}}{\dot{E}x_{g,in}^{ch} + \dot{E}x_{S3}^{ph}}$
Solution heat exchanger	$\dot{E}x_{S2}^{ph} + \dot{E}x_{S4}^{ph} = \dot{E}x_{S3}^{ph} + \dot{E}x_{S5}^{ph} + \dot{E}D_{she}^{ph}$	$\psi_{she} = \frac{\dot{E}x_{S3}^{ph} + \dot{E}x_{S5}^{ph}}{\dot{E}x_{S2}^{ph} + \dot{E}x_{S4}^{ph}}$
Absorber	$\dot{E}x_{R6}^{ph} + \dot{E}x_{S6}^{ph} + \dot{E}x_{W1}^{ph} = \dot{E}x_{S1}^{ph} + \dot{E}x_{W2}^{ph} + \dot{E}D_{abs}^{ph}$	$\psi_{abs} = \frac{\dot{E}x_{S1}^{ph} + \dot{E}x_{W2}^{ph}}{\dot{E}x_{R6}^{ph} + \dot{E}x_{S6}^{ph} + \dot{E}x_{W1}^{ph}}$
Evaporator	$\dot{E}x_{R4}^{ph} + \dot{E}x_{a,in}^{ph} = \dot{E}x_{a,out}^{ph} + \dot{E}x_{R5}^{ph} + \dot{E}D_{evap}^{ph}$	$\psi_{evap} = \frac{\dot{E}x_{a,out}^{ph} + \dot{E}x_{R5}^{ph}}{\dot{E}x_{R4}^{ph} + \dot{E}x_{a,in}^{ph}}$
Solution pump	$\dot{E}x_{S1}^{ph} + P_{sp} = \dot{E}x_{S2}^{ph} + \dot{E}D_{sp}^{ph}$	$\psi_{sp} = \frac{\dot{E}x_{S2}^{ph}}{\dot{E}x_{S1}^{ph} + P_{sp}}$
Condenser	$\dot{E}x_{R1}^{ph} + \dot{E}x_{W2}^{ph} = \dot{E}x_{R2}^{ph} + \dot{E}x_{W3}^{ph} + \dot{E}D_{cond}^{ph}$	$\psi_{cond} = \frac{\dot{E}x_{R2}^{ph} + \dot{E}x_{W3}^{ph}}{\dot{E}x_{R1}^{ph} + \dot{E}x_{W2}^{ph}}$

3.4. Economic analysis

From Fig. 1, it can be found that heat exchangers are the most significant parts of the AGAHP system. Because their heat transfer area affects their capital investment, a suitable design of heat exchangers could contribute to improve economic performance of the system. In this study, the heat transfer area of heat exchangers was defined by Equation 21.

$$A_{total} = A_{gen} + A_{cond} + A_{abs} + A_{evap} + A_{he} + A_{she} \quad (21)$$

The heat transfer area required by heat exchangers to transfer certain heat load could be expressed by Equation 22.

$$A = \frac{\dot{Q}}{U \Delta T_{LMTD}} \quad (22)$$

where ΔT_{LMTD} is the logarithmic mean temperature difference, calculated by Equation 23, for different flow arrangements.

$$\begin{aligned} \Delta T_{LMTD} &= \frac{(t_{h.in} - t_{c.out}) - (t_{h.out} - t_{c.in})}{\ln \frac{t_{h.in} - t_{c.out}}{t_{h.out} - t_{c.in}}} && \text{counter-current flow} \\ \Delta T_{LMTD} &= \frac{(t_{h.in} - t_{c.in}) - (t_{h.out} - t_{c.out})}{\ln \frac{t_{h.in} - t_{c.in}}{t_{h.out} - t_{c.out}}} && \text{parallel flow} \end{aligned} \quad (23)$$

The economic analysis was applied to estimate the capital investment and payback period, with the balance of cost rate calculated by Equation 24 [30].

$$\overset{\square}{C}_{total} = \overset{\square}{C}_g + \overset{\square}{C}_{env} + \overset{\square}{Z}_{op} + \overset{\square}{Z}_k \quad (24)$$

$$\overset{\square}{C}_{total} = (\overset{\square}{C}_g + \overset{\square}{C}_{env} + \overset{\square}{Z}_{op} + \overset{\square}{Z}_k) \times 3600 \times N \quad (25)$$

$$\overset{\square}{C}_g = 0.1444 \rho \cdot NP \cdot \frac{Q_{gen} / \eta_b}{36 \times 10^3} \quad (26)$$

$$\overset{\square}{C}_h = \frac{\overset{\square}{C}_{total}}{Q_{cond} + Q_{abs} + Q_{he-I}} \quad (27)$$

where $\overset{\square}{C}_g$ and $\overset{\square}{C}_{total}$ are natural gas cost rate and total cost rate, respectively. $\overset{\square}{C}_h$ is unit cost for heating. $\overset{\square}{Z}_{op}$ is the operational cost rate that can be described by

Equation 28.

$$\dot{Z}_{op} = \frac{\dot{P}_{sp} \times EP}{3600} \quad (28)$$

where \dot{P}_{sp} is the power of solution pumps and EP is the unit electricity price.

According to [31], the capital investment and maintenance costs of the system were defined by Equation 29.

$$\dot{Z}_k = C_{index} \times \frac{Z_k \times \phi}{N \times 3600} \times CRF \quad (29)$$

where Z_k is the capital investment of the equipment which is shown in Table 6. The capital cost of components is estimated by cost functions which must be converted from the reference year to the current year by using cost index factor. For this purpose, a systematic methodology is used to calculate the cost index factor using the Chemical Engineering Plant Cost Index (CEPCI) of the reference year and the current year, as given below [32].

$$C_{index} = \frac{CEPCI_{2020}}{CEPCI_{2012}} \quad (30)$$

where $CEPCI_{2020}$ is 650 and $CEPCI_{2012}$ is 583 [33]. The profit (Pr) of the system can be calculated as:

$$Pr = (\dot{Q}_{cond} + \dot{Q}_{abs} + \dot{Q}_{he-l}) \times HP \times 3600 \quad (31)$$

Sanaye reported the connecting pipes, refrigerant and system structure accounted only for 0.84% of gross investment [34,35]. Therefore, their cost were neglected and only the cost of EEV, heat exchangers and solution pump were considered. ϕ was the maintenance factor and CRF was the capital recovery factor, calculated by Equation 32 [36].

$$CRF = \frac{i(1+i)^n}{(1+i)^n - 1} \quad (32)$$

Table 6 Cost function of main equipment in 2016 [37]

Components	Z_k
Heat exchangers	$1397 \times A^{0.89}$
EEV	$114.5 \times m$

With the growing concerns about global warming and environmental pollution, the rate of penalty cost of CO₂ emission should be considered, as defined by Equation 33 [37,38].

$$C_{env} = \mu_{co_2} \times EC \times c_{co_2} + e_{co_2} \times A_{heating} \times c_{co_2} \quad (33)$$

where μ_{co_2} and c_{co_2} are CO₂ avoid cost and factor of emission, respectively. EC is system annual electrical energy consumption. e_{co_2} is CO₂ emissions of gas-fired boiler and $A_{heating}$ is heating area.

3.5. Multi-objective optimization

It is a problem that system payback period and exergy destruction are conflicting with each other. Therefore, the MOP method has been applied in this study as it can achieve optimization of the AGAHP system based on two objectives at the same time [30]. The ED and the PP have been selected as the objective functions in this study, as calculated by Equations 34 and 35, respectively.

$$ED_{total} = ED_{evap} + ED_{cond} + ED_{abs} + ED_{gen} + ED_{she} + ED_{he} + ED_{sp} \quad (34)$$

$$PP = \frac{Z_k \times 3600 + (C_g + C_{env} + Z_{op}) \times n \times 3600}{(Q_{cond} + Q_{abs} + Q_{he-l}) \times HP} \quad (35)$$

In this study, three optimization cases were considered, and they were ED single objective optimization, PP single objective optimization and MOP. The variables which can maximize or minimize the ED and PP were chosen as decision variables [20], and they were evaporating temperature and generator temperature. The constraints consist of both equality and inequality constraints. Equality constraints are formulated with solution and energy models, and inequality constraints permit the operational conditions inside safe limitations. The proposed AGAHP had two decision variables and the constraints were optimized by the NSGA-II technology, which is an effective method to look for optimal solutions of MOP, introduced by Deb in 2002 [39]. The details of the NSGA-II technology and its pseudo codes can be found in [20]. There are numerous non-dominated solutions namely Pareto frontier, in which any value of the objective functions cannot be improved without lowering some other objective values [40]. Therefore, a decision-making method is necessary to look for optimal solutions from the Pareto frontier. According to [41], it is necessary for both ED and PP to be in normalized form but not their actual values. In addition, the following fuzzy method can be used to conduct the non-dimensionalization process of the ED and the PP, as defined by Equations 36 and 37.

$$ED_i^n = \frac{\max(ED_i) - ED_i}{\max(ED_i) - \min(ED_i)} \quad (36)$$

$$PP_i^n = \frac{\max(PP_i) - PP_i}{\max(PP_i) - \min(PP_i)} \quad (37)$$

To identify optimal solutions, the TOPSIS decision-making method was used during the MOP process. The method includes both ideal point and non-ideal point, with ideal point minimizing the ED and the PP, while non-ideal point maximizing the ED and the PP. The distance of any points on the Pareto frontier from the ideal and non-ideal points could be measured by [Equations 38](#) and [39](#).

$$d_{i+} = \sqrt{(ED_i^n - ED^{n,ideal})^2 + (PP_i^n - PP^{n,ideal})^2} \quad (38)$$

$$d_{i-} = \sqrt{(ED_i^n - ED^{n,non-ideal})^2 + (PP_i^n - PP^{n,non-ideal})^2} \quad (39)$$

The proximity index of this method can be calculated by [Equation 40](#)[42].

$$Cl_i = \frac{d_{i-}}{d_{i+} + d_{i-}} \quad (40)$$

If both ED and PP were ideal points of the Pareto frontier, Cl_i would be 1. If they were non-ideal points, Cl_i would be 0. Finally, the point with maximum Cl_i was chosen as the optimal result, with the MOP flowchart shown in [Fig. 5](#).

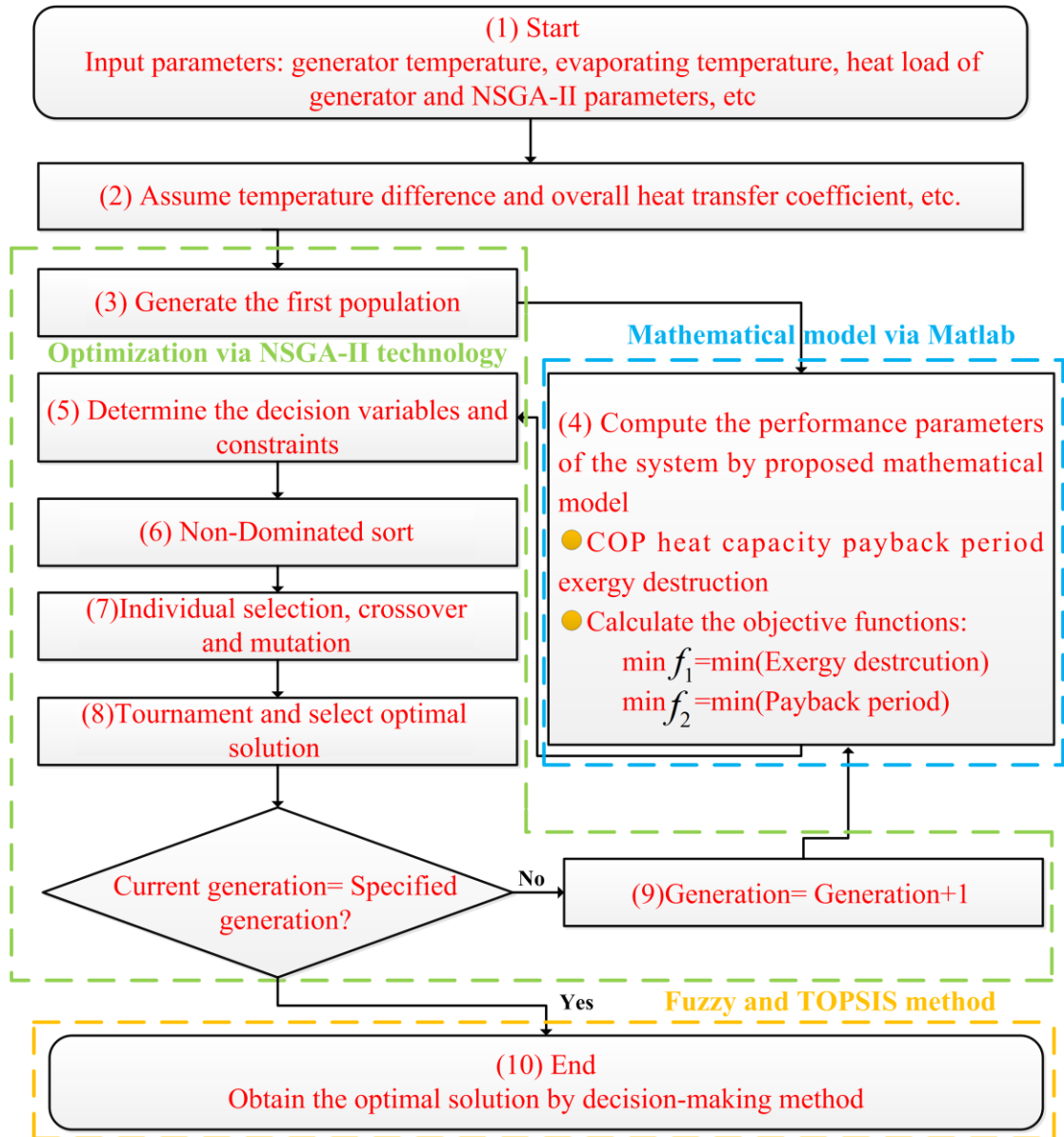


Fig. 5 Multi-objective optimization flowchart

4. Results and discussions

The AGAHP system is aiming to provide district heating for users in cold regions. In this section, a case study was conducted to analyze both the thermodynamic and the economic performances of AGAHP systems, using the mathematical model proposed above. The heat capacity of the system was designed as 40 kW and the temperatures of supply water and return water were set as 45 °C and 35 °C, respectively. Table 7 has listed major thermodynamic conditions of the AGAHP system, and Table 8 has listed detailed parameters applied in the economic analysis.

Table 7 Thermodynamic conditions of the AGAHP

Simulation parameters	Values
Generator temperature (°C)	190

Evaporating temperature (°C)	-20
Absorption temperature (°C)	43
Condensing temperature (°C)	46
Supply water temperature (°C)	45
Return water temperature (°C)	35
Heat load of generator (kW)	27
Inlet temperature of air (°C)	-5
Outlet temperature of air (°C)	-10
Percent excess air (%)	20
Degree of superheating of refrigerant at evaporator outlet (°C)	0
Overall heat transfer coefficient of the condenser [W/(m ² ·K)]	1200 [43]
Overall heat transfer coefficient of the evaporator [W/(m ² ·K)]	30 [43]
Overall heat transfer coefficient of the absorber [W/(m ² ·K)]	1000 [43]
Overall heat transfer coefficient of the generator [W/(m ² ·K)]	100 [43]
Boiler efficiency (%)	0.88

Table 8 Economic model parameters [44]

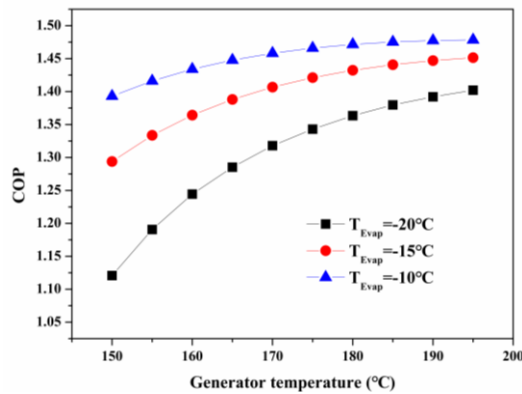
Parameters	Value
Maintenance factor φ	1.06
Annual interest rate i (%)	15
The system life time n (year)	15
Annual operational hours N (h)	3600
Average of electricity price in China EP [\$(kW·h)]	0.11 [45]
Average of heat price in China HP [\$(kW·h)]	0.08 [45]
Natural gas price in China NP (\$/kg)	0.4909 [6]
Emission factor of electricity in China μ_{co_2} (kg/kWh)	0.88
Cost of CO ₂ avoided c_{co_2} (\$/ton)	87 [45]
CO ₂ emission of gas-fired boiler e_{co_2} (kg/m ²)	21.89 [38]
Heating area $A_{heating}$ (m ²)	1000

4.1. Thermodynamic performance

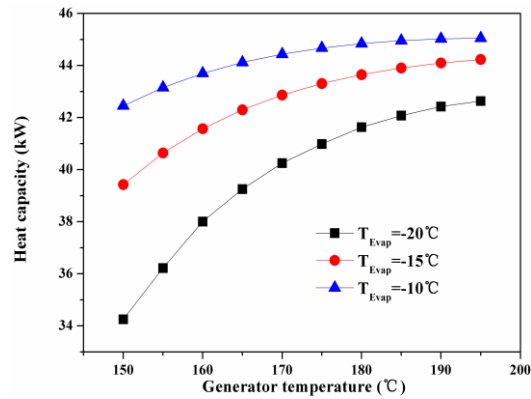
The energy analysis mainly consisted of COP, heat capacity, exergy destruction and efficiency. Fig. 6(a) displays the calculated system's COP, with generator temperature set with different evaporating temperatures. It reflects that the system's COP increased with increasing generator temperature, when the evaporating temperature was kept as a constant. When the generator temperature became stable, the COP increased with the increasing evaporating temperature. When the generator temperature was 195 °C, the COP was 1.41 at the evaporating temperature of -20 °C,

1.45 at the evaporating temperature of $-15\text{ }^{\circ}\text{C}$ and 1.48 at the evaporating temperature of $-10\text{ }^{\circ}\text{C}$, respectively. This is because that higher generator temperature leads to lower weak solution concentration. As the strong solution concentration kept unchanging, the increase of deflation ratio caused the increase of absorption ability. Both mass flow rate of refrigerant and heat capacity of condenser were then increased, resulting in increased COP. From Fig. 6(b), it could be observed that the heat capacity rose with increasing generator and evaporating temperatures. When the generator temperature was $195\text{ }^{\circ}\text{C}$, the heat capacity was 42.62 kW at the evaporating temperature of $-20\text{ }^{\circ}\text{C}$, 44.23 kW at the evaporating temperature of $-15\text{ }^{\circ}\text{C}$ and 45.05 kW at the evaporating temperature of $-10\text{ }^{\circ}\text{C}$. The increase of evaporating temperature lead to rising evaporating pressure and then to increased absorber pressure. This resulted in higher deflation ratio, which gave more heat capacity.

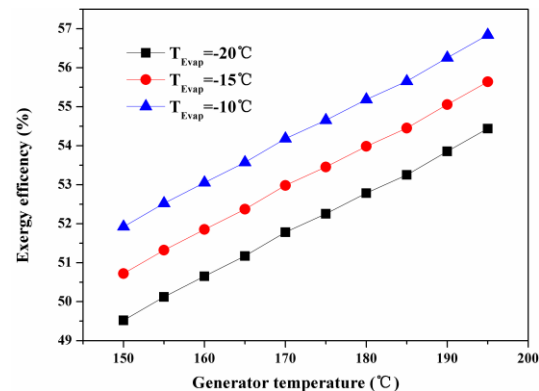
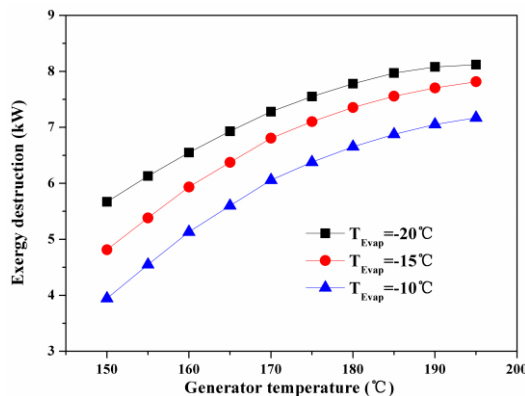
Figs. 6(c) and 6(d) illustrate the variation of exergy destruction calculated by Equation (15) and efficiency calculated by Equation (20), under different generator temperatures and evaporating temperatures. From the results, it could be found that both exergy destruction and efficiency increased with increasing generator temperature, when the evaporating temperature was kept as constant. When the generator temperature was $195\text{ }^{\circ}\text{C}$, the exergy destruction was 8.12 kW at the evaporating temperature of $-20\text{ }^{\circ}\text{C}$, 7.81 kW at the evaporating temperature of $-15\text{ }^{\circ}\text{C}$ and 7.17 kW at the evaporating temperature of $-10\text{ }^{\circ}\text{C}$. A higher evaporating temperature has led to a lower exergy destruction and higher exergy efficiency, as the temperature difference between evaporator and ambient temperatures decreased.



(a)



(b)



(c)

(d)

Fig. 6 Energy and exergy performances of the system

4.2. Economic performance

Fig. 7 displays the economic performance of the AGAHP system under different conditions. Fig. 7(a) shows that a longer life time and a lower interest rate could lead to a lower CRF. When life time was longer than 10 years, the reduction rates of CRF were almost constant with different interest rates. Fig. 7(b) indicates that with the increase of generator temperature, the capital investment would increase because of the increase of heat capacity, which led to increased heat transfer area. A higher evaporating temperature lead to a higher heat capacity, which caused a higher capital investment. From Fig. 7(c), the profit of the AGAHP system increased with increase of generator temperature as heat capacity rose. The profit calculated by the denominator of Equation (35) determined the system's profit. When the generator temperature was 195 °C, the maximum profit at the evaporating temperature of -20 °C, -15 °C and -10 °C were 12278 \$, 12379 \$ and 12974 \$, respectively. Fig. 7(d) has depicted the variation of system's payback period, which was calculated by Equation (35). When the generator temperature increased from 150 °C to 195 °C, the payback period decreased from 6.89 years to 5.73 years, at the evaporating temperature of -20 °C, from 6.06 years to 5.55 years at the evaporating temperature of -15 °C, and from 5.67 years to 5.46 years at the evaporating temperature of -10 °C. The payback period was relatively long because of the consideration of natural gas and operation maintenance. This could be explained by that the growth rate of capital investment and operation maintenance cost were less than the growth rate of profit. Fig. 7(e) displays the tendency of unit cost of heating with the generator temperature. Under the different evaporating temperature, the unit cost of heating increased with the increase of generator temperature. When the generator temperature increased from 150 °C to 195 °C, the unit cost of heating increased from 10.55 \$/GJ to 14.77 \$/GJ, at the evaporating temperature of -20 °C, from 10.58 \$/GJ to 14.74 \$/GJ at the evaporating temperature of -15 °C, and from 10.59 \$/GJ to 14.74 \$/GJ at the evaporating temperature of -10 °C. According to the Ref. [45], the heat price was 0.08 \$/kWh which could be convert to 22.23 \$/GJ. Compared with conventional district heating, AGAHP has better economic performance.

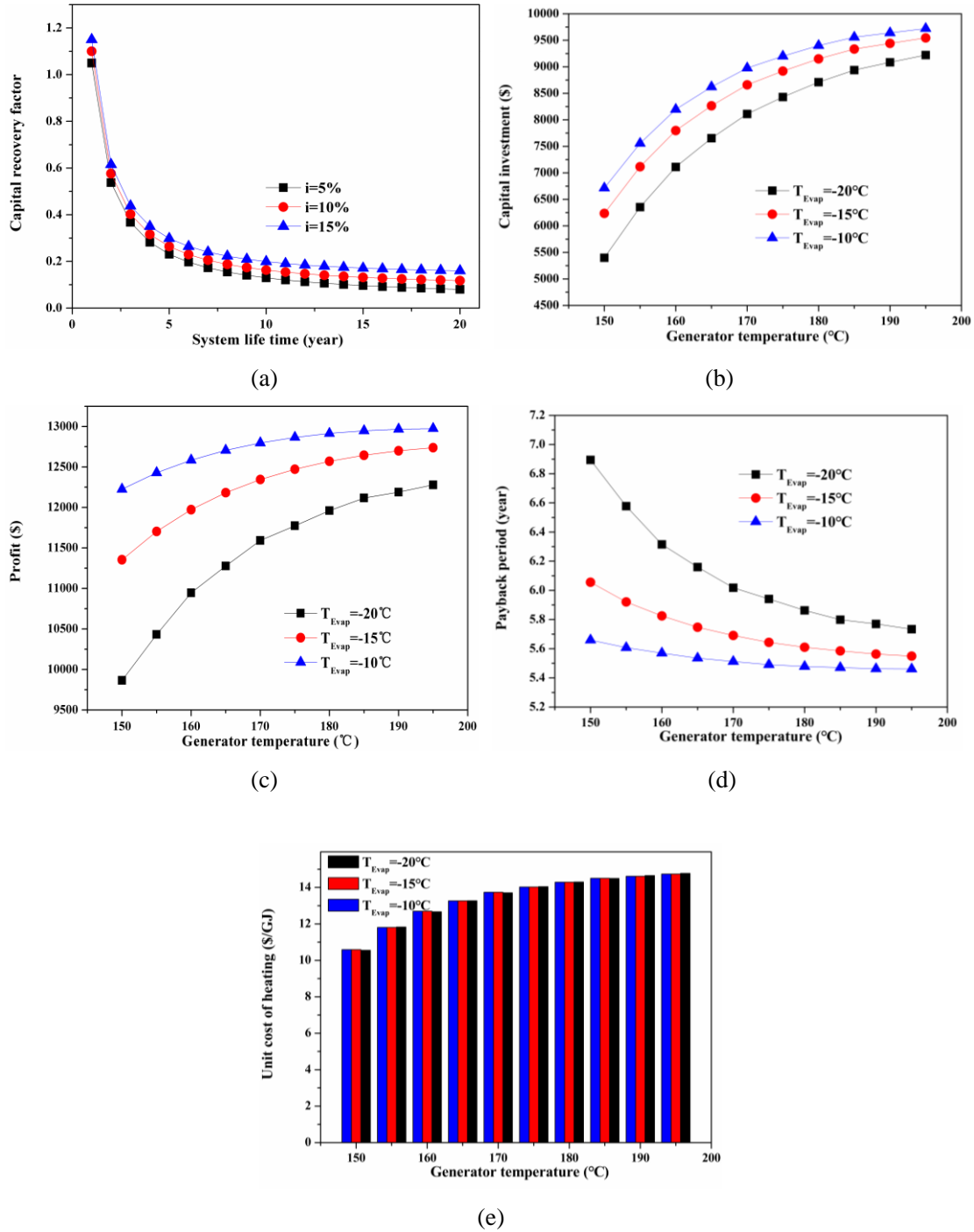


Fig. 7 Economic performance of the system

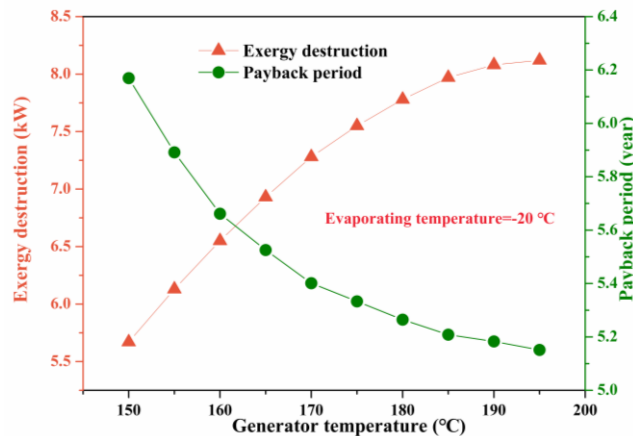
4.3. System optimization

The MOP of the AGAHP system was done using the NSGA-II technology and the TOPSIS decision-making method. The tuning parameters used in the MOP have been listed in Table 9, adopted from [20] when using the MOP method to a vapor absorption heat transformer system.

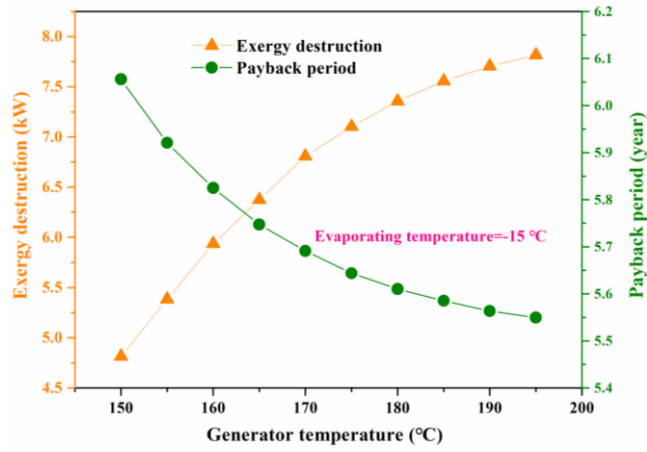
Table 9 Tuning Parameters in MOP [20]

Tuning parameters	Value
Population size	100
Maximum number of generations	400
Probability of crossover	0.9
Probability of mutation	0.1
Selection process	Tournament
Tournament size	2

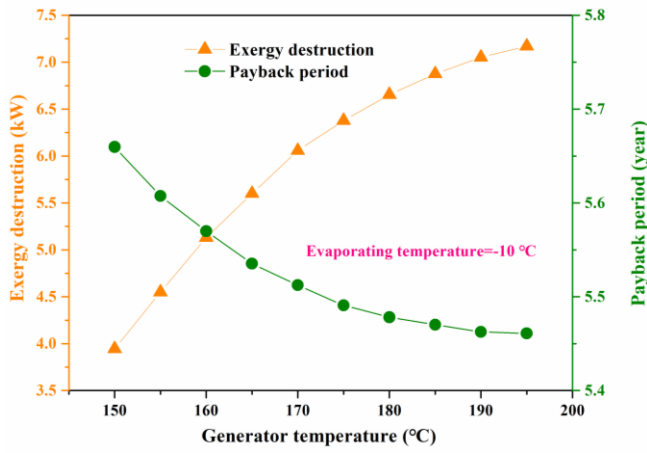
Fig. 8 shows both exergy destruction and payback period of the AGAHP at various conditions. As shown in Figs. 8(a), 8(b) and 8(c), the ED increased and the PP decreased with increasing generator temperature. As aforementioned, a system with small ED may have long PP, and a system with short PP may have big ED, so both are not optimal. This issue was solved in this study using the multi-objective optimization method. According to Equations. (36-39), the Pareto frontiers with normalized form using the NSGA-II technology in MOP are shown in Figs. 9 (a), 9(b) and 9(c), for different working conditions. Normalized PP and normalized ED were calculated according to Equations (36) and (37). When the condensing temperature was $-10\text{ }^{\circ}\text{C}$, $-15\text{ }^{\circ}\text{C}$ and $-20\text{ }^{\circ}\text{C}$, the maximum and minimum PP and ED could be collected from Fig. 7(a) to calculate the normalized payback period and normalized exergy destruction in every point. From Figs. 9(a), 9(b) and 9(c), it is shown that the ideal point could be found when the normalized ED and the normalized PP were 1. According to Equations (36) and (37), both ED and PP were minimal under this condition. However, it needs to be noted that the existence of this ideal point is not practically possible. The non-ideal point was found when the normalized ED and the normalized PP were 0. When the normalized ED was 1 and the normalized PP was 0, the system was an ED-based optimal design. When the normalized ED was 0 and the normalized PP was 1, the system was a PP-based optimal design. To find the optimal solution in the Pareto frontier, the TOPSIS decision-making method was also applied.



(a)

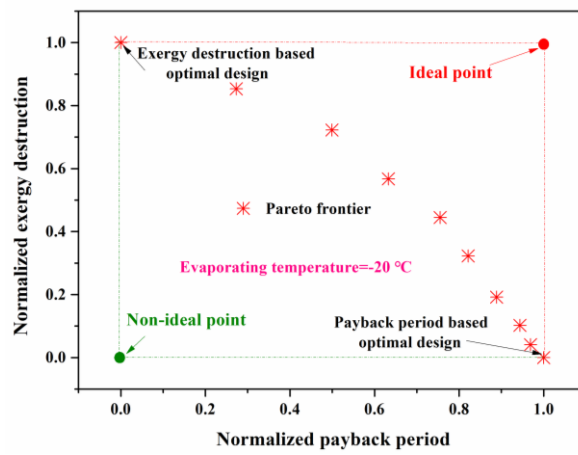


(b)

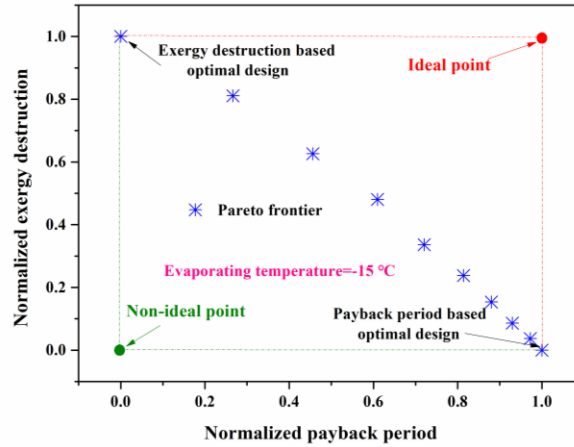


(c)

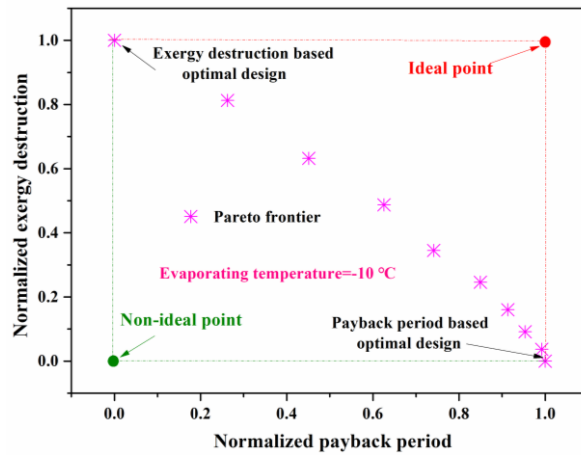
Fig. 8 Exergy destruction and payback period of the system



(a)



(b)



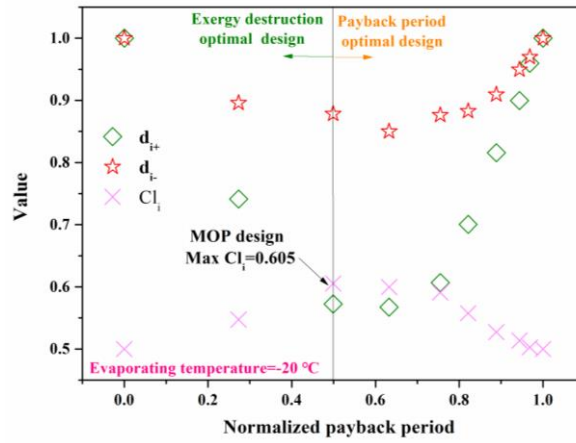
(c)

Fig. 9 Pareto frontier with normalized form in MOP process

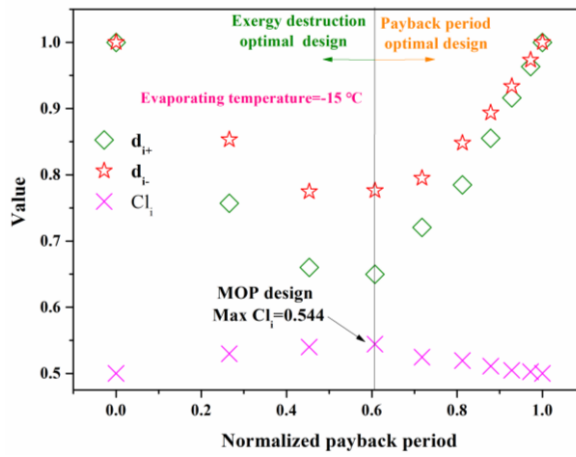
According to the Equations (38-40), the d_{i+} , d_{i-} and Cl_i of every point were calculated and a point with the maximum proximity index Cl_i has been selected as the final result. Fig. 9 shows the variation of d_{i+} , d_{i-} and Cl_i with normalized PP. It indicated that both d_{i+} and d_{i-} decreased firstly and then started to increase under different working conditions. The Cl_i was calculated by d_{i+} and d_{i-} and it increased at the beginning and then started to decrease. From Fig. 10(a), it could be found that the maximum Cl_i was 0.605 at the normalized PP of 0.499, when the generator temperature was 160 °C. In this optimal solution, the PP was 6.31 years and the ED was 6.35 kW, when the evaporating temperature was -20 °C. From Fig. 10(b), it can be observed that the maximum Cl_i was 0.544 at the normalized PP of 0.609,

when the generator temperature was 165 °C. When the evaporating temperature was -15 °C, the optimal PP and the optimal ED were 5.75 years and 6.37 kW, respectively. According to Fig. 10(c), the maximum Cl_i was 0.555 at the normalized PP of 0.625, when the generator temperature was 165 °C. The optimal PP and the optimal ED were 5.53 years and 5.59 kW, when the evaporating temperature was -10 °C. As shown in Fig. 10, any points of the Pareto frontier located on the left hand side of the maximum Cl_i had better exergy performance. Those points located on the right hand side, however, had better economic performance.

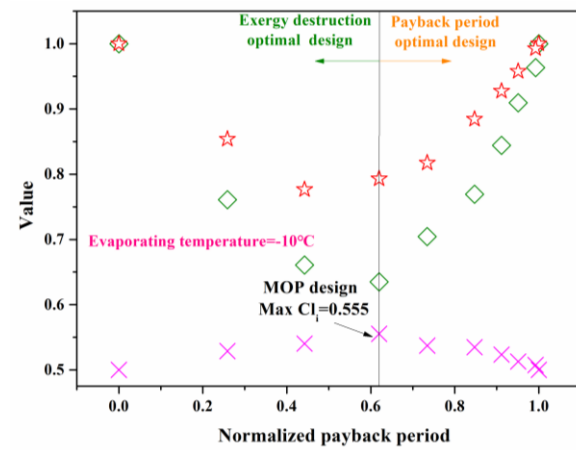
Table 10 shows ED, normalized ED, PP and normalized PP in both SOP and MOP procedures. It should be noted that if any of the PP based optimized design (SOP of PP) or ED based optimized design (SOP of ED) was selected, the design would inadequately meet other conditions. According to Table 11, if the SOP of PP was chosen as optimal design, the average ED was 37.87 % higher than its minimum possible value; whereas, if the SOP of ED was chosen, the average PP was 11.12 % higher than its minimum possible value. In addition, if the MOP design is selected as the final solution, the average ED and PP are 4.51 % and 5.07 % more than their minimum possible values. Therefore, MOP design is more favorable than the other SOP designs. Additionally, when the evaporating temperature was -20 °C, all COP, exergy destruction and payback period were poorer than those with evaporating temperature at -15 °C and -10 °C. When the evaporating temperature was -10 °C, however, the system's performance became worse in severe cold areas. Fig. 11 shows the results from the exergy analysis of the optimal condition and some thermodynamic parameters concerned with system performance at evaporating temperature of -15 °C were listed in Table 11. It reflected in Fig. 11 that generator was the biggest contributor to the ED, caused by the large temperature difference.



(a)



(b)



(c)

Fig. 10 The values in TOPSIS method

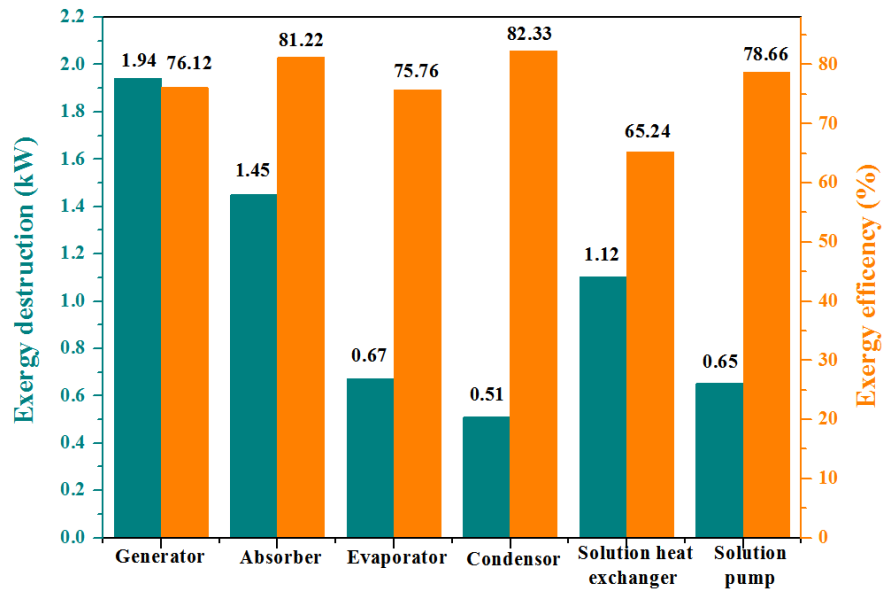


Fig. 11 Exergy analysis of the system under optimal condition at the evaporating temperature of $-15\text{ }^{\circ}\text{C}$

Table 10 ED and PP value under three optimization procedure

Optimization parameters	ED_{total} (kW)			PP (year)			ED_i^n			PP_i^n		
Evaporating temperature (°C)	-20	-15	-10	-20	-15	-10	-20	-15	-10	-20	-15	-10
Design conditions	8.12	7.81	7.17	5.73	5.55	5.46	0	0	0	1	1	1
SOP of ED	5.67	4.81	3.94	6.89	6.06	5.65	1	1	1	0	0	0
MOP	6.35	6.37	5.59	6.31	5.75	5.53	0.72	0.48	0.49	0.50	0.61	0.63
SOP of PP	8.12	7.81	7.17	5.73	5.55	5.46	0	0	0	1	1	1

Table 11 Thermodynamic conditions in different processes

Parameter	MOP conditions
Q_{evap} (kW)	10.69
Q_{cond} (kW)	16.35
Q_{gen} (kW)	27.34
Q_{abs} (kW)	21.07
COP	1.39
\square Z_k (\$/s)	5.61E-4
PP (year)	5.16
ED (kW)	6.37

5. Conclusions

In this study, a novel air-source gas-fired absorption heat pump system for heating with flue gas recovery has been proposed. The performance of the AGAHP has been evaluated and analyzed, considering aspects including energy, exergy, economy and environment. For analyzing the effects of generator temperature and evaporating temperature on the thermodynamic and economic performance of the system, a mathematical model has been developed. Both multi-objective optimization and TOPSIS decision-making method have been adopted to find optimal design and operation states of the AGAHP system, with minimized exergy destruction and payback period. Main findings from this study have been summarized as followings,

1. For the system proposed in this study, its COP, heat capacity, exergy destruction and efficiency, capital investment and profit would all increase with increasing generator temperature, but not for payback period. When generator temperature was 195 °C, the maximized COP and heat capacity were 1.48 and 45.05 kW, respectively, at evaporating temperature of -10 °C;
2. A lower exergy destruction of the system may lead to longer payback period, and vice versa. Both are not optimal design. When the generator temperature was 195 °C, the maximum profit and minimum payback period were 12974 \$ and 5.46 years, respectively.
3. The system can be optimized by solving the conflict between payback period and exergy destruction, using the multi-objective optimization method. Through this optimization work, if the MOP design was selected as the final solution, the average ED and the average PP were 4.51 % and 5.07 % higher than their minimum possible values, respectively. This optimization work gave better

performance than the single-objective optimization.

Acknowledgement

This work was supported by the Natural Science Foundation of Tianjin (No. 19JCQNJC07200) and National Key R&D Program of China (No. 2018YFC0705000)

References

- [1] Wu ZX, Zhang YF, He ZL et al. Performance investigation of a bi-functional integration system for power and heat supply. *Applied thermal engineering* 148(2019) 714-721.
- [2] Halit A, Oguz A. Exergoeconomic analysis of district heating system boosted by the geothermal heat pump. *Energy* 119(2017) 1159-1170.
- [3] Mahdi De, Sajjad V, Ahmad A. Simultaneous use of air-side and water-side economizers with the air source heat pump in a data center for cooling and heating production. *Applied thermal engineering* 161(2019) 114113.
- [4] Qiu JY, Zhang H, Sheng J et al. Experimental investigation of L41b as replacement for R410A in a residential air-source heat pump water heater. *Energy and buildings* 199(2019) 190-196.
- [5] Li SH, Gong GC, Peng JQ. Dynamic coupling method between air-source heat pumps and buildings in China's hot-summer/cold-winter zone. *Applied energy* 254(2019) 113664.
- [6] Lu D, Chen GF, Gong MQ et al. Thermodynamic and economic analysis of a gas-fired absorption heat pump for district heating with cascade recovery of flue gas waste heat. *Energy Conversion and Management* 185 (2019) 87-100.
- [7] Wu W, Wang BL, You T et al. Configurations of solar air source absorption heat pump and comparisons with conventional solar heating. *Applied thermal engineering* 141(2018) 630-641.
- [8] Dai EQ, Jia T, Dai YJ. Theoretical and experimental investigation on a GAX-Based ammonia-water absorption heat pump driven by parabolic trough solar collector. *Solar energy* 197(2020) 498-510.
- [9] Li XT, Wu W, Zhang XL et al. Energy saving potential of low temperature hot water system based on air source absorption heat pump. *Applied thermal engineering* 2012;48:317-324.
- [10] Wu W, Shi WX, Wang BL et al. A new heating system based on coupled air source absorption heat pump for cold regions: Energy saving analysis. *Energy Conversion and Management*. 76(2013)811-817.
- [11] Christopher M.K, Srinivas G, Michael A.G. Modeling of an ammonia-water absorption heat pump water heater for residential applications. *International Journal of Refrigeration* 83(2017) 39-50.

- [12]Lu D, Bai Y, Zhao YX et al. Experimental investigations of an absorption heat pump prototype with intermediate process for residential district heating. *Energy Conversion and Management* 204 (2020) 112323.
- [13]Wang YL, Liu YG, Liu XB et al. Advanced exergy and exergoeconomic analyzes of a cascade absorption heat transformer for the recovery of low grade waste heat. *Energy Conversion and Management* 205 (2020) 112392.
- [14]Luca U, Daniele T. Integration of reversible absorption heat pumps in cogeneration systems:Exergy and economic assessment. *Energy Conversion and Management* 200 (2019) 112062.
- [15]Li X, Wang ZF, Yang M et al. Proposal and performance analysis of solar cogeneration system coupled with absorption heat pump. *Applied Thermal Engineering* 159(2019) 113873.
- [16]Bellos E, Tzivanidis C. Parametric analysis and optimization of a solar driven trigeneration system based on ORC and absorption heat pump. *Journal of Cleaner Production* 161(2017) 493-509.
- [17]Rodrigue L, Paiguy A, Brigitte A et al. Exergetic, ecological and thermo-economic (3E) optimization of an absorption heat pump with heat resistance, heat leakage and two internal irreversibilities: Comparison. *International Journal of Refrigerant* 112(2020) 251-261.
- [18]Evangelos B, Christos T. Parametric analysis and optimization of a solar driven trigeneration system based on ORC and absorption heat pump. *Journal of Cleaner Production* 53(2017) 26-36.
- [19]Jia T, Dai EQ, Dai YJ. Thermodynamic analysis and optimization of a balanced-type single-stage ammonia-water absorption-resorption heat pump cycle for residential heating application. *Energy* 171(2019) 120-134.
- [20]Vaibhav J, Gulshan S. Energy, exergy, economic (3E) analyzes and multi-objective optimization of vapor absorption heat transformer using NSGA-II technique. *Energy Conversion and Management* 148 (2017) 1096-1113.
- [21]Qu Ming, Omar A, Yin HX. New configurations of a heat recovery absorption heat pump integrated with a natural gas boiler for boiler efficiency improvement. *Energy Conversion and Management* 87 (2014) 175-184.
- [22]Yuan H, Zhang J, Huang XK et el. Experimental investigation on binary ammonia-water and ternary ammonia-water-lithium bromide mixture-based absorption refrigeration systems for fishing ships. *Energy Conversion and Management* 166(2018)13-22.
- [23]Nico M, Fabian S, Bernd B et al. Design and analysis of an ammonia-water absorption heat pump. *Applied Thermal Engineering* 165(2020) 114531.
- [24]Arif L. Yearly simulation of a solar-aided R22-DEGDME absorption heat pump system. *Solar energy* 55(195) 255-265.
- [25]You SJ. Studies on the R22-DEGDME absorption heat pump cycles. Master. Tianjin University, Tianjin, China, 1985. (In Chinese)
- [26]Ando E, Takcshito I. Residential gas-fired absorption heat pump based on R22-DEGDME Pair, Part 1: thermodynamic properties of R22-DEGDME Pair. *International Journal of Refrigeration* 7(1984) 181-185.

- [27] Takeshito I, Yamamoto Y, Harada T et al. Residential gas-fired absorption heat pump based on R22-DEGDME Pair, Part 2: design, computer simulation and testing of a prototype. *International Journal of Refrigeration* 7(1984) 313-321.
- [28] Wu ZX, Zhang YF, Sheng Y. Energy, exergy, economic(3E) analysis and multi-objective optimization of a novel dual functional integration system. *Energy Conversion and Management* 199 (2019) 111962.
- [29] Carlos M, Joaquin N, Adrión Mota et al. Experimental exergy and energy analysis of a novel high-temperature heatpump with scroll compressor for waste heat recovery. *Applied Energy* 253(2019) 113504.
- [30] Wu ZX, Sha L, Zhao MZ et al. Performance analyzes and optimization of a reverse Carnot cycle-organic Rankine cycle dual-function system. *Energy Conversion and Management* 212 (2020) 112787.
- [31] Mahdi N, Ali S, Sepehr S. Four E analysis and multi-objective optimization of an ice storage system incorporating PCM as the partial cold storage for air-conditioning applications. *Applied Thermal Engineering* 58(2013) 30-41.
- [32] Muhammad A, Muhammad W, Syed M. A comprehensive framework for thermoeconomic analysis of desalination systems. *Energy Conversion and Management* 222(2020)113188.
- [33] Dimitri Mignard. Correlating the chemical engineering plant cost index with macro-economic indicators. *Chemical Engineering Research and Design*, 92 (2014) 285-294.
- [34] Sanaye S, Malekmohammadi H. Thermal and economical optimization of air conditioning units with vapor compression refrigeration system. *Applied Thermal Engineering* 24(2004) 1807-1825.
- [35] Wu ZX, Sha L, Yang XC et al. Performance evaluation and working fluid selection of combined heat pump and power generation system (HP-PGs) using multi-objective optimization. *Energy Conversion and Management* 221 (2020) 113164.
- [36] Bejan A, Tsatsaronis G, Moran MJ. *Thermal design and optimization*. Wiley; 1996.
- [37] Mosaffa AH, Farshi LG, Ferreira CAI et al. Exergoeconomic and environmental analyzes of CO₂/NH₃ cascade refrigeration systems equipped with different types of flash tank intercoolers. *Energy Conversion and Management* 117(2016)442-453.
- [38] Zhao J, Duan YQ, Liu XJ. Study on the policy of replacing coal-fired boilers with gas-fired boilers for central heating based on the 3E system and the TOPSIS method: A case in Tianjin, China. *Energy* 189(2019) 116206.
- [39] Deb K, Pratap A, Agarwal S, Meyarivan T. A fast and elitist multi-objective genetic algorithm: NSGA-II. *IEEE Transactions Evolutionary Computation* 2002;6:182–197.
- [40] Wang YZ, Zhao J, Wang Y et al. Multi-objective optimization and grey relational analysis on configurations of organic Rankine cycle. *Applied Thermal Engineering* 114(2017) 1355-1363.
- [41] Sayyaadi H, Nejatolahi M. Multi-objective optimization of a cooling tower

- assisted vapor compression refrigeration system. *International Journal of Refrigeration* 34(2011) 243-256.
- [42]Wu ZX, Wang YR, You SJ et al. Thermo-economic analysis of composite district heating substation with absorption heat pump. *Applied thermal engineering* 166(2020) 114659
- [43]Roetzel W, Spang B. C3 typical values of overall heat transfer coefficients. Berlin Heidelberg: Springer-Verlag; 2010.p.75-78.
- [44]Mosaffa AH, Farshi LG, Ferreira CAI et al. Exergoeconomic and environmental analyzes of CO₂/NH₃ cascade refrigeration systems equipped with different types of flash tank intercoolers. *Energy Conversion and Management* 117(2016)442-453.
- [45]Sayyaadi H, Nejatolahi M. Efficiency enhancement of a gas turbine cycle using an optimized tubular recuperative heat exchanger. *Energy* 38(2012) 362-75.